SYNTHESIS AND CHARACTERIZATION OF LITHIUM-SUBSTITUTED BIOGLASS-CERAMIC POWDERS

Mihai FOTU[1], Ștefan MANOLACHE[2] Adrian-Ionuț NICOARĂ[3], Cristina BUSUIOC[4*]

The growing demand for bone substitutes has led to significant advancements in bone tissue engineering. In this study, lithium-substituted bioglass-ceramics were synthesized using the sol-gel method, valued for its efficiency and the production of materials with high surface area and nanoporosity. The powders calcined at 600 °C were characterized through Thermogravimetric Analysis, Fourier Transform Infrared Spectroscopy, X-ray Diffraction and Raman spectroscopy, as well as Scanning Electron Microscopy and Energy Dispersive Spectroscopy analyses. Thermogravimetric analysis revealed increased residual mass and enhanced thermal stability due to lithium compounds. X-ray Diffraction revealed a crystalline structure dominated by combeite and minor phases of calcium sodium phosphate and silicon oxide. Fourier Transform Infrared Spectroscopy and Raman analyses confirmed lithium integration into the structural network, inducing compositional and structural modifications. These findings suggest that lithium substitution improves the properties of the materials, making these ceramics promising for bone regeneration applications.

Keywords: bioglass-ceramics, lithium substitution, sol-gel method, structural characterization, bone tissue engineering

1. Introduction

Bone diseases and injuries are a major global health concern, affecting millions of people annually. Conditions such as osteoporosis, fractures, and congenital bone defects require effective solutions for bone regeneration. Current treatments include autografts, allografts, and synthetic materials, but each has limitations. Traditional biomaterials, such as metals and polymers, often fail to promote tissue integration or bioactivity, necessitating the development of advanced materials that actively support bone healing. Bioactive glasses or glass-

[1] PhD Student, Department of Science and Engineering of Oxide Materials and Nanomaterials, Faculty of Chemical Engineering and Biotechnologies, National University of Science and Technology POLITEHNICA Bucharest, Romania, e-mail: mihai.fotu@stud.chimie.upb.ro

[2] MSc Student, Faculty of Medical Engineering and Biotechnologies, National University of Science and Technology POLITEHNICA Bucharest, Romania, e-mail: stefan.manolache@stud.fim.upb.ro

[3] Assoc. Prof., Department of Science and Engineering of Oxide Materials and Nanomaterials, Faculty of Chemical Engineering and Biotechnologies, National University of Science and Technology POLITEHNICA Bucharest, Romania, e-mail: adrian.nicoara@upb.ro

[4*] Prof., Department of Science and Engineering of Oxide Materials and Nanomaterials, Faculty of Chemical Engineering and Biotechnologies, National University of Science and Technology POLITEHNICA Bucharest, Romania, corresponding author, e-mail: cristina.busuioc@upb.ro

ceramics are a category of materials predominantly used in bone tissue engineering and dentistry [1], playing a crucial role in fracture repair and other tissue healing processes. These materials can bond to bone surface, forming an apatite layer that initiates biomineralization [2], thereby accelerating the bone remodeling process. Bioactive glass is typically classified into three forms based on its composition: silicate (SiO_2), phosphate (P_2O_5), and borate (B_2O_3), each exhibiting distinct properties and applications. Due to their amorphous structure, they can bond with both hard and soft tissues, making them suitable for applications such as tendon or cartilage repair as well [3-5].

In 1969, Larry Hench discovered bioactive glass, a material that bonded with tissue and supported its healing [6,7]. Over the next 40 years, extensive research transitioned from materials that interact with tissue to those that support and even stimulate cellular growth. During this period, bioactive glass became the gold standard in bone tissue engineering while continuing to be studied and improved, leading to the development and patenting of new formulations [8-10]. *In vivo* tests showed that bioactive glass outperforms synthetic hydroxyapatite in promoting bone cell proliferation, making it a top choice for bone remodeling scaffolds. It can be used alone, in composites, or with natural bone to stimulate growth, and can be applied as a powder or paste for filling fractures, dental canals, or strengthening the maxilla for implants [8,11]. Patented as Bioglass® or 45S5 Bioglass, this silicon-based glass contains 45 % silica and a Ca:P ratio of 5:1. For biocompatibility and bioactivity, it requires 43–47 % SiO_2, 22.5–26.5 % CaO and Na_2O, and 5–7 % P_2O_5, all as mass ratios [9].

Larry Hench used the melt-derived method to synthesize bioactive glass by mixing and melting silicon, calcium, sodium, and phosphorus oxides at 1100–1300 °C. The molten glass was poured into platinum molds to prevent contamination and underwent thermal treatments [11]. The sol-gel method is favoured for its simplicity, low processing temperatures, and precise control of material properties. It forms a gel from metal salt solutions via hydrolysis and condensation, followed by drying and thermal treatment. This process enhances porosity, surface area, and osteointegration while enabling functionalization with ions, growth factors, or drugs to improve performance and reduce aggregation [8].

Bioactive glass regained prominence with late 20^{th} and early 21^{st} century technological advancements. The past two decades marked its golden age, with hundreds of studies published annually. As its properties became better understood, researchers explored alternative materials, developing new compositions within the Si−Ca−Na−P system [8,11,12]. These materials provide antimicrobial protection *in situ* and can be enhanced by metal substitution [13] (e.g., silver, which has antimicrobial properties; magnesium, which supports osteogenesis; copper, known for angiogenic effects; strontium, which promotes bone formation [2] and reduces resorption; or lithium, which enhances bone density and regeneration) or metallic

oxide coatings (e.g., zinc oxide, which has antibacterial effects; magnesium oxide, enhancing biocompatibility) [14,15]. Bioactive glass also serves as a dental remineralization agent, with S53P4 showing higher silica release, reduced decalcification, and better dentinal pore occlusion compared to traditional bioactive glass when applied to enamel-deficient teeth [16]. Studies showed that bioactive glass offers strong mineralization, excellent tissue adhesion, and superior durability compared to traditional glass, making it ideal for treating dentinal hypersensitivity, preventing caries, and depositing dental coatings [17]. Bioactive glasses are also used as controlled release systems for active substances, requiring biocompatibility, mechanical strength, and release capability [5]. Porous bioactive glasses meet these criteria, delivering growth factors to aid bone remodeling and drugs like anti-inflammatories or analgesics for post-surgery pain relief [14,18].

Although bioactive glasses can be modified with various metallic ions to enhance their biological and mechanical properties, lithium (Li^+) substitution has gained significant attention due to its unique benefits. Lithium salts, like carbonate, sulphate, or citrate, are used to treat severe depression, bipolar disorder, and mood swings [15,19,20]. Lithium is used in osteogenesis, bone remodeling [19], wound healing [19,20], and nerve regeneration, either as lithium chloride or carbonate, in composites, or as a substituted element in bioceramics and bioactive glasses. Lithium-substituted bioactive glasses exhibit increased density and a tendency to crystallize, forming phases such as Li_2SiO_3 and combeite ($Na_6Ca_3Si_6O_{18}$) [9,21].

In this study, we aim to develop lithium-substituted biovitroceramics and investigate the calcined powders obtained at 600 °C. The research is focused on assessing the influence of lithium substitution on the structural characteristics of bioactive glass, with an emphasis on its crystallization potential. To cover a diverse compositional range, lithium was introduced at mass concentrations of 2.5, 5, and 10%. These concentrations were chosen to replace calcium ions due to their comparable atomic size to lithium. The obtained materials were analysed using advanced structural and compositional characterization techniques to evaluate its potential for enhancing bone regeneration.

2. Materials and Methods

2.1 Experimental procedure

The experimental study started from a base bioglass whose composition contains 47.5 % SiO_2, 23.75 % CaO, 23.75 % Na_2O and 5 % P_2O_5. To obtain samples containing Li, CaO was replaced in proportions of 2.5, 5 and 10 wt%. These specific proportions were chosen for their similarity to established patented materials and to achieve a calcium-to-phosphorus molar ratio of 4.75, closely approximating the ideal value of 5 in conventional bioactive glass. This balance plays a key role in facilitating the formation of carbonated hydroxyapatite in bone and promoting new tissue regeneration.

The synthesis method chosen for preparing the samples was the sol-gel process and the necessary steps are presented in Fig. 1.

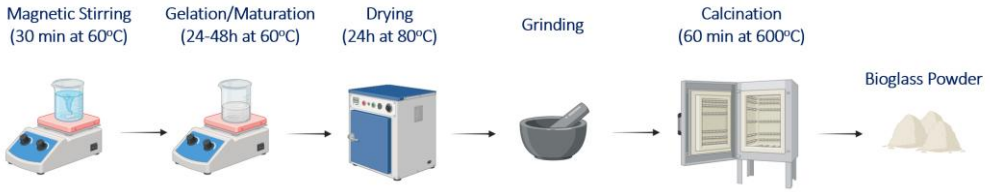

Fig. 1. Steps in the synthesis process of lithium-substituted bioactive glass powder using the sol-gel method.

Synthesis began with the dissolution of solid precursors—calcium nitrate tetrahydrate ($Ca(NO_3)_2 \cdot 4H_2O$, 98 % purity), sodium nitrate ($NaNO_3$, 99.8 % purity), and lithium sulphate (Li_2SO_4 99 % purity)—in distilled water and 99.5 % ethyl alcohol. The precursors were dosed and stirred for approximately 30 min at 60 °C on a magnetic plate until homogenized. Under continued magnetic stirring, liquid precursors were added dropwise: tetraethyl orthosilicate (TEOS – $Si(OC_2H_5)_4$, 98 % purity) and triethyl phosphate (TEP – $(C_2H_5O)_3PO$, 99 % purity).

The solution was stirred for about 1 h at 60 °C until it transitioned into a gel phase. The gel was then dried in an oven at 80 °C for 24 h. After complete evaporation of water, the product was removed from the oven, cooled, finely ground using a mortar and pestle, and calcined at 600 °C for 1 h. For obtaining lithium-substituted materials, the synthesis process followed the same steps as for simple bioglass, with the only modification being the adjusted quantities of calcium precursor (Table 1) added to the solutions.

Table 1.

Oxide composition of lithium-substituted bioglasses.

BG Type	***Composition (wt%)***				
	SiO_2	**P_2O_5**	**Li_2O**	**CaO**	**Na_2O**
BG	**47.5**	**5**	**0**	**23.75**	**23.75**
BG-2.5Li	**47.5**	**5**	**2.5**	**21.25**	**23.75**
BG-5Li	**47.5**	**5**	**5**	**18.75**	**23.75**
BG-10Li	**47.5**	**5**	**10**	**13.75**	**23.75**

Note: The coding for the samples reflects the lithium oxide (Li_2O) substitution level: "BG" represents the baseline composition without lithium, while "BG-2.5Li," "BG-5Li," and "BG-10Li" correspond to the incorporation of 2.5, 5, and 10 % Li_2O, respectively, replacing equivalent amounts of calcium oxide (CaO).

2.2 Characterisation Methods

Thermal analyses were performed in air using a Shimadzu DTG-TA-50H instrument (Carlsbad, USA) over a temperature range from room temperature to 900 °C to assess the thermal stability and decomposition behavior of the samples.

Chemical bond identification was carried out using Fourier-transform infrared spectroscopy (FT-IR) on a Nicolet iS50R spectrometer (Thermo Fisher, Waltham, MA, USA) with spectra collected at room temperature between 4000 and 400 cm^{-1} at a resolution of 4 cm^{-1}, employing an attenuated total reflection (ATR) module.

Raman spectroscopy was utilized at room temperature to study the local structural arrangement of the samples. The measurements were performed using a LabRAM HR Evolution spectrometer from Horiba (Japan). Raman spectra were obtained using a 514 nm argon-ion laser, focused on micrometer-sized areas of the samples, with a beam power of 125 mW, and a measurement error of ±0.5 cm^{-1}.

The structural properties were analysed using X-ray diffraction (XRD) at room temperature, in air, utilizing a PANalytical Empyrean system (Almelo, The Netherlands) equipped with a Cu X-ray tube (λ CuKα1 = 1.541874 Å). Scans were conducted across a 2θ range of 10–80 ° with 0.02 ° increments and a dwell time of 100 s per step.

Material morphology was examined through scanning electron microscopy (SEM) using a Quanta Inspect F50 microscope paired with an energy dispersive spectrometer (EDS) (Thermo Fisher, Eindhoven, The Netherlands). Grain size distribution was assessed via ImageJ 1.50i software (Wayne Rasband, National Institute of Health, Rockville, MD, USA, 2016).

3. Results and discussions

The analysis of the materials began with the characterization of powders calcined at 600 °C. This includes thermogravimetric analysis, as shown in Fig. 2 (a), which highlights the material mass losses. Additionally, Table 2 outlines the stages of these mass changes, expressed as a function of temperature and corresponding mass percentages.

From the data presented above, it can be observed that increasing the amount of lithium addition leads to a rise in the residual mass and a corresponding decrease in mass loss caused by the effect of temperature on the materials composition. This suggests an enhancement in the thermal resistance of the material, attributed to the formation of lithium-based compounds. The thermal analysis also includes the study of the differential scanning calorimetry curve, which provides insights into the thermal processes underlying the mass changes, as well as their endothermic or exothermic nature.

Fig. 2 (b) illustrates the thermal behaviour of the samples (BG, BG-2.5Li, BG-5Li, and BG-10Li) over a temperature range of 25 to 900°C. The curves show both endothermic and exothermic processes. Endothermic events, represented by dips below the baseline, occur primarily at lower temperatures, likely associated with the removal of adsorbed water or evaporation of volatile components.

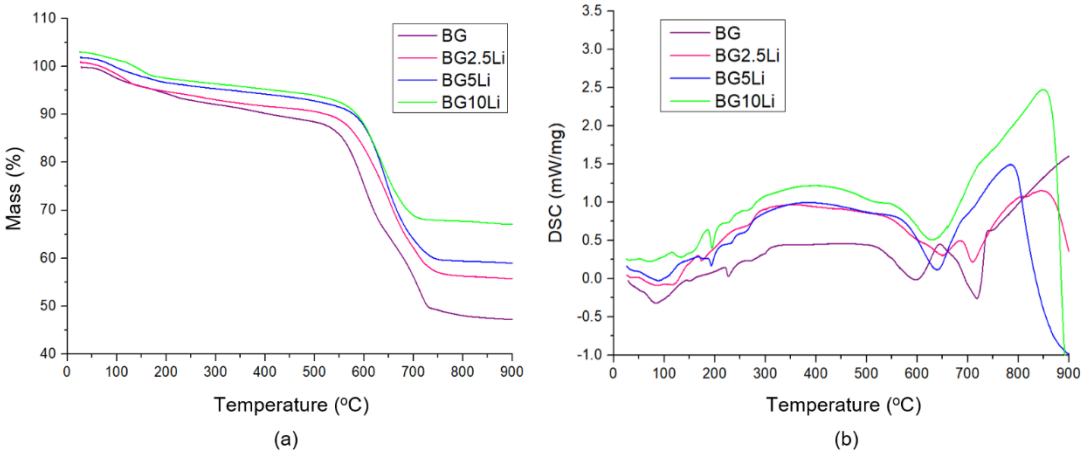

Fig. 2. Thermogravimetric analyses of the precursor gels (a) and the corresponding differential scanning calorimetry graphs (b).

Table 2.

Mass loss values during the thermogravimetric analysis.

BG type	***Mass changes (%)***		
	25-500 °C	**500-730 °C**	**Residual mass**
BG	11.52	41.25	47.23
BG-2.5Li	11.52	33.79	54.69
BG-5Li	10.46	32.56	56.98
BG-10Li	9.48	26.46	64.06

Exothermic processes, indicated by peaks above the baseline, are more pronounced at higher temperatures and correspond to structural transformations or crystallization events in the material. Notably, the intensity and position of these peaks vary with the lithium content, suggesting that lithium influences the thermal stability and phase transformations of the materials. Therefore, since lithium has been observed to enhance the thermal resistance of the material, it can be concluded that the exothermic processes are associated with phase transitions that contribute to structural improvement.

The X-ray diffraction patterns shown in Fig. 3 (a) reveals a crystalline structure with numerous peaks, distinct from the diffractogram of classical bioglass, indicating the formation of glass-ceramics. As the lithium concentration increases, certain peaks become more pronounced, suggesting a possible increase in the crystalline order or crystallinity of specific phases. The BG-5Li and BG-10Li samples exhibit the most intense peaks, implying a higher degree of crystallinity in these samples compared to BG and BG-2.5Li [12].

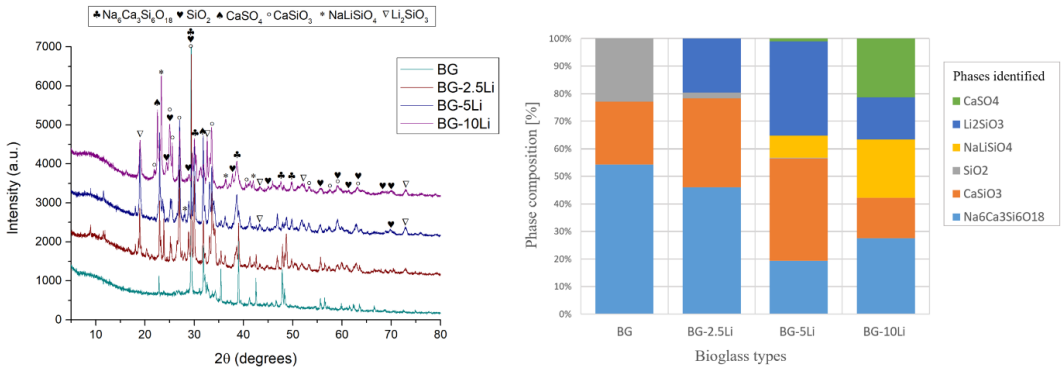

Fig. 3. XRD patterns of bioglass samples (BG, BG-2.5Li, BG-5Li and BG-10Li) (a) and their XRD-determined phase compositions (b).

The presence of $Na_6Ca_3Si_6O_{18}$ (ICDD 04-012-8759), a sodium-calcium silicate phase, indicates that bioactive silicate structures are preserved, ensuring their role in ion exchange and hydroxyapatite formation [22]. Meanwhile, the formation of $NaLiSiO_4$ (ICDD 04-016-0897) indicates the successful incorporation of lithium ions into the matrix, potentially replacing sodium and reorganizing the silicate framework. An increase in the amount of calcium sulphate (ICDD 00-003-0163) was observed, which could potentially enhance regenerative properties and support biological integration in biomedical applications [12]. Additionally, the lithium-specific Li_2SiO_3 (ICDD 00-029-0828) phase is more prominent in the BG-5Li and BG-10Li samples, highlighting lithium active interaction with the glass structure and its potential to alter the material characteristics.

Fig. 3 (b) presents the phase composition of lithium-substituted bioglasses, determined through Rietveld refinement of XRD data. The unsubstituted BG sample is dominated by $Na_6Ca_3Si_6O_{18}$ and $CaSiO_3$ (ICDD 04-009-5600), while lithium incorporation leads to the formation of $NaLiSiO_4$ and Li_2SiO_3, indicating structural changes. In BG-10Li, the presence of $CaSO_4$ suggests further phase evolution. These results highlight the impact of lithium substitution on the crystalline structure, which may influence the material properties.

The FTIR spectra, presented in Fig. 4, demonstrate the effects of lithium substitution on the bioglass structure.

The Si–O stretching band around ~1000 cm^{-1} intensifies in BG-5Li and BG-10Li, indicating a more stable and ordered silicate network. The P–O bending band near ~500 cm^{-1} reaches its maximum intensity in BG-5Li, but a slight reduction is observed in BG-10Li. This suggests that a moderate lithium concentration (5 %) enhances phosphate integration into the bioglass network, while higher concentrations may reduce this effect.

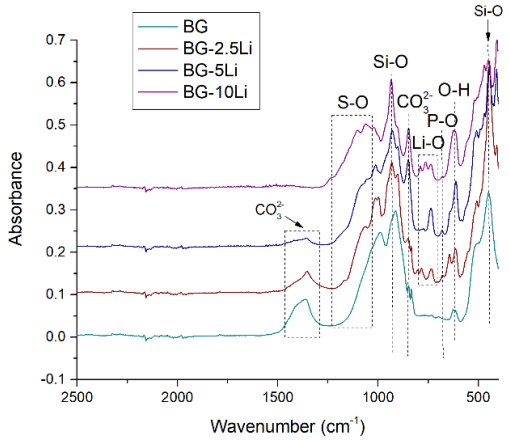

Fig. 4. The FT-IR spectra of bioglass samples (BG, BG-2.5Li, BG-5Li and BG-10Li).

Phosphate is critical for bioactivity and plays a key role in interactions with bone tissue.

Additionally, a distinct band around ~700-800 cm^{-1}, associated with Li^+ ions, is prominent in BG-5Li and BG-10Li, confirming the successful incorporation of lithium ions into the bioglass matrix. The ~1400 cm^{-1} band, attributed to CO_3^{2-} ions, also shows its highest intensity in BG-5Li, followed by a decrease in BG-10Li, indicating that moderate lithium levels optimize carbonate group formation. According to the Raman analysis (Fig. 5), the band in the 200-400 cm^{-1} range is attributed to Ca-O bonds [23,24], which are essential for the bioactivity of the material.

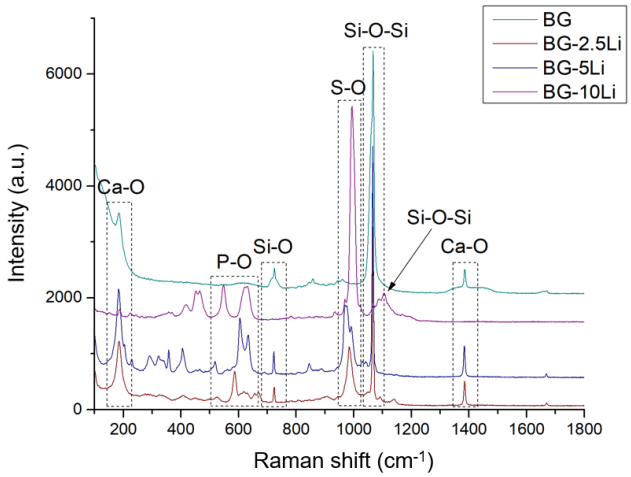

Fig. 5. Raman spectra of bioglass samples (BG, BG-2.5Li, BG-5Li and BG-10Li).

In the 800-1200 cm^{-1} range, characteristic bands of the silicate [25,26] network (Si–O and Si–O–Si) are observed, reflecting the fundamental structure of

the bioglass. Additionally, a band around 1000 cm^{-1}, associated with S−O bonds [25,26], may indicate possible impurities or the presence of additional components in the composition.

Lithium substitution introduces visible changes in the spectrum. At a 2.5 % concentration (BG-2.5Li), the fundamental bioglass structure remains mostly unchanged, with minor variations in the intensity of the Si−O bands. At 5 % concentration (BG-5Li), the Si−O−Si band intensifies, while the Ca−O and P−O bands show slight attenuation, suggesting that lithium begins to influence the structural network by increasing its degree of order. At the maximum concentration of 10 % (BG-10Li), the Si−O−Si signal becomes highly defined, indicating that lithium significantly contributes to the ordering of the silicate network.

Concurrently, a slight reduction in the intensity of the Ca−O and P−O bands may suggest a redistribution of these elements within the bioglass matrix [15].

These observations suggest that lithium substitution affects both the chemical structure and physical properties of bioglasses. Increasing lithium concentration appears to favour a more ordered silicate network, which could have positive implications for the medical applications of these materials, such as enhanced bioactivity and improved interaction with bone tissues [21].

Fig. 6 shows the SEM images of the samples treated at 600 ºC at a magnification of ×25,000.

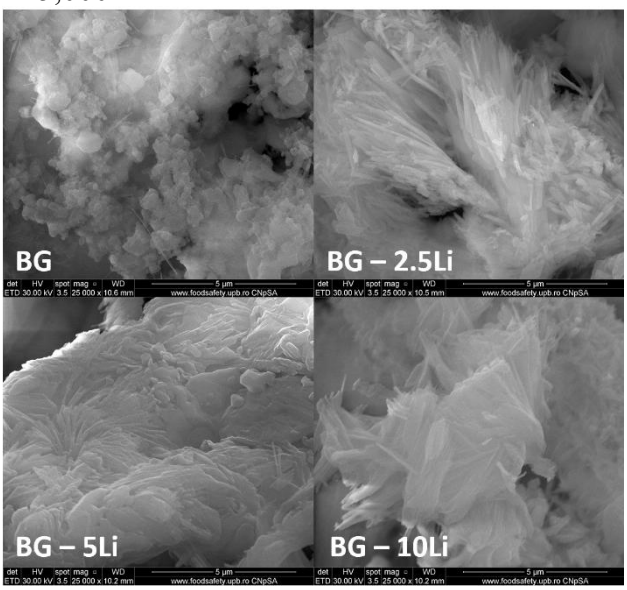

Fig. 6. SEM images (magnification ×25,000) of bioglass samples (BG, BG-2.5Li, BG-5Li and BG-10Li).

The images reveal significant morphological changes as the lithium content increases. The BG sample (unsubstituted) exhibits an aggregated morphology with irregular particles (1–5 μm) and a rough surface of the aggregates, features

commonly associated with partially crystalline materials. In BG-2.5Li, acicular and fibrillar entities begin to emerge, suggesting that lithium substitution promotes partial crystallization, with increased local network ordering. For BG-5Li, the acicular morphology becomes more pronounced, forming radial or fascicular crystal bundles, with lithium facilitating lamellar-acicular domain development. Finally, BG-10Li shows dense fibrous aggregates and a strongly acicular morphology, likely representing advanced crystallization or the formation of lithium-rich phases, such as lithium silicates [27,28].

The EDS spectra of samples BG, BG-2.5Li, BG-5Li and BG-10Li are shown in Fig. 7. All the spectra indicate the presence of the following characteristic elements: oxygen (O), sodium (Na), silicon (Si) and calcium (Ca). For the samples substituted with 2.5, 5 and 10 % lithium, the presence of sulphur (S) is observed.

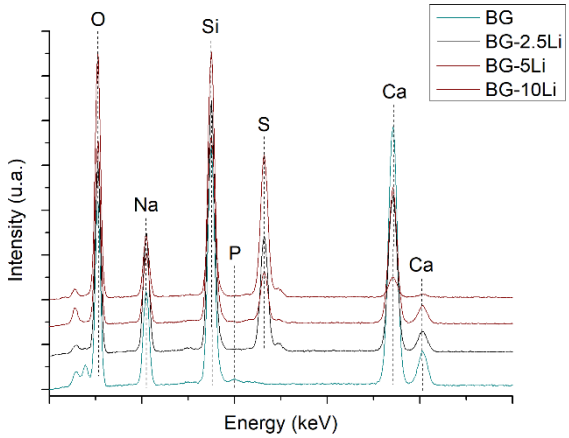

Fig. 7. EDS spectra of bioglass samples (BG, BG-2.5Li, BG-5Li and BG-10Li).

4. Conclusions

The analysis of bioglass samples calcined at 600 °C highlights the significant influence of lithium substitution on their thermal, structural, and morphological properties. Thermogravimetric analysis showed that higher lithium content improves thermal resistance, leading to increased residual mass and reduced mass loss due to lithium-based compound formation. XRD analysis revealed the transition to a glass-ceramic structure, with increased crystallinity and pronounced peaks for lithium-substituted samples, indicating enhanced order within the silicate network. The stabilization of phases like $Na_6Ca_3Si_6O_{18}$ and $NaLiSiO_4$, along with the presence of Li_2SiO_3, underscores lithium role in structural modifications. FTIR and Raman analyses confirmed lithium integration into the bioglass matrix, shown by shifts in vibrational bands. Increased Si–O–Si and P–O band intensity indicates a more ordered network, while Li^+-specific bands reveal direct structural interaction. The SEM analysis demonstrated that increasing lithium content induces significant morphological transformations, transitioning from an amorphous,

irregular microstructure in bioglass to a highly acicular and fibrous morphology in the bioglass substituted with the highest percentage of Li. This evolution suggests that lithium substitution enhances crystallization, leading to the formation of ordered lamellar-acicular domains and potential lithium-rich phases.

These findings underscore the potential of lithium-substituted bioglass powders for biomedical applications, particularly in bone tissue engineering, where enhanced crystallinity and bioactivity are crucial for improved performance. Mechanical properties represent a crucial aspect of future research, as they are fundamental for both the biological function of bone and the performance of scaffolds intended for its regeneration. Although this study focuses on structural and morphological characterization, the findings underscore the need for further research on the mechanical properties and bioactivity of lithium-substituted bioglasses for bone tissue engineering.

Acknowledgement

The authors are grateful to the Romanian Government for providing access to the research infrastructure of the National Centre for Micro and Nanomaterials through the National Program titled “Installations and Strategic Objectives of National Interest”.

R E F E R E N C E S

[1] Atia GAN, Mohamed SZ, Halim HA, Ghobashy MM, Foda T, Shalaby HK, et al. Advances in Bioceramic silicates for therapeutic, and regenerative Dentofacial reconstruction. Ceram Int 2024;50:22184–208. https://doi.org/10.1016/j.ceramint.2024.04.035.

[2] Li XC, Lu XT, Bai T, Yang H, Li D, Chen M, et al. Mechanical behavior and biological activity performance of Li+/Ca2+@Li+/K+ ion-exchanged lithium disilicate glass-ceramics. Ceram Int 2024. https://doi.org/10.1016/j.ceramint.2024.09.066.

[3] Kaou MH, Furkó M, Balázsi K, Balázsi C. Advanced Bioactive Glasses: The Newest Achievements and Breakthroughs in the Area. Nanomaterials 2023;13. https://doi.org/10.3390/nano13162287.

[4] Balasubramanian P, Büttner T, Miguez Pacheco V, Boccaccini AR. Boron-containing bioactive glasses in bone and soft tissue engineering. J Eur Ceram Soc 2018;38:855–69. https://doi.org/10.1016/j.jeurceramsoc.2017.11.001.

[5] Krishnan L, Chakrabarty P, Govarthanan K, Rao S, Santra TS. Bioglass and nano bioglass: A next-generation biomaterial for therapeutic and regenerative medicine applications. Int J Biol Macromol 2024;277. https://doi.org/10.1016/j.ijbiomac.2024.133073.

[6] Hench LL. Opening paper 2015- some comments on bioglass: Four eras of discovery and development. Biomedical Glasses 2015;1:1–11. https://doi.org/10.1515/bglass-2015-0001.

[7] Hench LL, Polak JM. Third-Generation Biomedical Materials. Science (1979) 2002;295:1014–7. https://doi.org/10.1126/science.1067404.

[8] Rahaman MN, Day DE, Sonny Bal B, Fu Q, Jung SB, Bonewald LF, et al. Bioactive glass in tissue engineering. Acta Biomater 2011;7:2355–73. https://doi.org/10.1016/j.actbio.2011.03.016.

[9] Deliormanlı AM, Yıldırım M. Sol-gel synthesis of 13-93 bioactive glass powders containing therapeutic agents. vol. 52. 2016.

[10] Drago L, Toscano M, Bottagisio M. Recent evidence on bioactive glass antimicrobial and antibiofilm activity: A mini-review. Materials 2018;11. https://doi.org/10.3390/ma11020326.

[11] Krishnan V, Lakshmi T. Bioglass: A novel biocompatible innovation. J Adv Pharm Technol Res, vol. 4, Wolters Kluwer Medknow Publications; 2013, p. 78–83. https://doi.org/10.4103/2231-4040.111523.
[12] Gomez Gramajo F, Rivoira MA, Rodríguez V, Vargas G, Vera Mesones R, Zago MP, et al. Lithium-containing 45S5 Bioglass-derived glass-ceramics have antioxidant activity and induce new bone formation in a rat preclinical model of type 1 diabetes mellitus. Biomedical Materials 2025;20:015006. https://doi.org/10.1088/1748-605X/ad8c8b.
[13] Chromčíková M, Hruška B, Nowicka A, Macháček J, Liška M. Thermal properties and thermodynamic model of lithium doped 45S5 bioglass. J Therm Anal Calorim 2023. https://doi.org/10.1007/s10973-023-12668-2.
[14] Mortazavi V, Mehdikhani Nahrkhalaji M, Fathi MH, Mousavi SB, Nasr Esfahani B. Antibacterial effects of sol-gel-derived bioactive glass nanoparticle on aerobic bacteria. J Biomed Mater Res A 2010;94:160–8. https://doi.org/10.1002/jbm.a.32678.
[15] Khorami M, Hesaraki S, Behnamghader A, Nazarian H, Shahrabi S. In vitro bioactivity and biocompatibility of lithium substituted 45S5 bioglass. Materials Science and Engineering C 2011;31:1584–92. https://doi.org/10.1016/j.msec.2011.07.011.
[16] Forsback AP, Areva S, Salonen JI. Mineralization of dentin induced by treatment with bioactive glass S53P4 in vitro. Acta Odontol Scand 2004;62:14–20. https://doi.org/10.1080/00016350310008012.
[17] Salonen Jl, Arjasmaa M, Tuominen U, Behbehani MJ, Zaatar El. Bioactive glass in dentistry. Journal Of Minimum Intervention In Dentistry 2009:1–12.
[18] Méndez JA, Fernández M, González-Corchón A, Salvado M, Collía F, De Pedro JA, et al. Injectable self-curing bioactive acrylic-glass composites charged with specific anti-inflammatory/analgesic agent. Biomaterials 2004;25:2381–92. https://doi.org/10.1016/j.biomaterials.2003.09.004.
[19] Tondo L, Alda M, Bauer M, Bergink V, Grof P, Hajek T, et al. Clinical use of lithium salts: guide for users and prescribers. Int J Bipolar Disord 2019;7. https://doi.org/10.1186/s40345-019-0151-2.
[20] Ruffalo ML. A Brief History of Lithium Treatment in Psychiatry. Prim Care Companion CNS Disord 2017;19. https://doi.org/10.4088/PCC.17br02140.
[21] Farmani AR, Salmeh MA, Golkar Z, Moeinzadeh A, Ghiasi FF, Amirabad SZ, et al. Li-Doped Bioactive Ceramics: Promising Biomaterials for Tissue Engineering and Regenerative Medicine. J Funct Biomater 2022;13. https://doi.org/10.3390/jfb13040162.
[22] Norouzi A, Banijamali S, Keshavarzi A. Sinter-crystallization, phase development and microstructural evaluations of ZnO containing 45S5 ® glass-ceramics. vol. 5. 2018.
[23] Gavinho SR, Hammami I, Jakka SK, Teixeira SS, Silva JC, Borges JP, et al. Influence of the Addition of Zinc, Strontium, or Magnesium Oxides to the Bioglass 45S5 Network on Electrical Behavior. Materials 2024;17. https://doi.org/10.3390/ma17020499.
[24] Rehman I, Hench LL, Bonfield W, Smith R. Analysis of surface layers on bioactive glasses. n.d.
[25] Stan GE, Bojin D. ADHERENT GLASS-CERAMIC THIN LAYERS WITH BIOACTIVE POTENTIAL DEPOSITED BY MAGNETRON SPUTTERING TECHNIQUES. Bull, Series B 2010;72.
[26] González P, Serra J, Liste S, Chiussi S, León B, Pérez-Amor M. Raman spectroscopic study of bioactive silica based glasses. J Non Cryst Solids 2003;320:92–9. https://doi.org/10.1016/S0022-3093(03)00013-9.
[27] Subha P V., Nair BN, Hareesh P, Mohamed AP, Yamaguchi T, Warrier KGK, et al. Enhanced CO2 absorption kinetics in lithium silicate platelets synthesized by a sol-gel approach. J Mater Chem A Mater 2014;2:12792–8. https://doi.org/10.1039/c4ta01976h.
[28] Soares VO, Serbena FC, Mathias I, Crovace MC, Zanotto ED. New, tough and strong lithium metasilicate dental glass-ceramic. Ceram Int 2021;47:2793–801. https://doi.org/10.1016/j.ceramint.2020.09.133.